Int. J. Electrochem. Sci., 14 **(2019)** 4161 – 4172, doi: 10.20964/2019.05.44

International Journal of
ELECTROCHEMICAL
SCIENCE
www.electrochemsci.org

High Performance Sn–In Cathode for the Electrochemical Reduction of Carbon Dioxide to Formic Acid

Fajun Li[1,2], *Hua Zhang*[1], *Shuai Ji*[1], *Wei Liu*[3], *Dong Zhang*[1], *Chengdu Zhang*[1], *Jing Yang*[1], *Fei Yang*[1], *Lixu Lei*[1,2,*]

[1] School of Chemistry and Chemical Engineering, Southeast University, Nanjing 211189, China
[2] The Jiangsu Key Laboratory for Advanced Metallic Materials, Nanjing, 211189, China
[3] Key Laboratory of Electrochemical Energy Storage Technology of Jiangsu Province, Shuangdeng Group Co. Ltd. Taizhou, Jiangsu 225300, China
[*]E-mail: lixu.lei@seu.edu.cn

Received: 3 January 2019 / *Accepted:* 1 March 2019 / *Published:* 10 April 2019

Both Sn and In have been potentiostatically co-deposited on the surface of Cu foam at different potentials to prepare Sn–In bimetallic electrodes. Among them, the $Sn_{42}In_{58}$ electrode has excellent catalytic activity towards CO_2 reduction to formic acid. At −1.6 V versus Ag/AgCl, the formate Faradaic efficiency reaches its maximum, 88%; and its space time yield reaches 309 μmol h^{-1} cm^{-2} at −1.8 V versus Ag/AgCl. When it is used in the biomimetic electrochemical cell reported previously by us, a much higher space time yield, 468 μmol h^{-1} cm^{-2} is obtained.

Keywords: Electrochemical reduction, carbon dioxide, formate, tin–indium bimetallic catalyst, space time yield

1. INTRODUCTION

The increasing consumption of fossil fuels and its consequent concern of climate change have led to considerable interest in the utilisation of CO_2.[1-4] CO_2 can be utilised and recycled into abundant carbon feedstocks through chemical methods,[5-8] however, the electrochemical reduction of CO_2 ($ERCO_2$) at a heterogeneous metal surface in an aqueous solution is more promising[9,10] because it can selectively produce carbonaceous compounds and oxygen, similar to photosynthesis of plants, especially when the electricity used comes from photovoltaic cells. The compounds produced, such as formic acid and CO, can be selectively controlled by changing the electrode material and electrolyte;[11] and financial and feasibility analyses conclude that it could be run with profits.[12]

Formic acid is a liquid at ambient temperature, and plays a crucial role in industry, such as pharmaceutical synthesis, textile finishing and animal feed additives.[13] In addition, it is the fuel for

direct formic acid fuel cells,[14-18] and a hydrogen storage material.[19] Formic acid can be easily obtained through electrochemical reduction of CO_2 on Cd, In, Sn, Tl, and Pb electrodes.[20] Particularly, formic acid obtained through electrochemical reduction of CO_2 at Sn electrodes has been reported with excellent Faradaic efficiencies and space time yields. However, there is still need on improving them.

The first thing is to improve the Faradaic efficiency (FE) and space time yield (STY), by using electrodes with high overpotential for hydrogen evolution reaction (HER), and high specific area for $ERCO_2$. For example, Lv reported that a Sn plate electrode produces formic acid at a current density of 2.5 mA cm^{-2} (36 μmol h^{-1} cm^{-2}) with FE of approximately 78%,[21] and a Sn deposited on Cu foil electrode produces formic acid at a current density of 5.8 mA cm^{-2} (99 μmol h^{-1} cm^{-2}) with FE of approximately 91.5%,[22] however, if Sn is deposited on Cu foam electrode, higher average current density (8 mA cm^{-2}, 124 μmol h^{-1} cm^{-2}) and FE (83.5%) were obtained.[23] The oxide layer on Sn electrode is very important for the high FE, as it makes HER more difficult.[24] Gas diffusion electrodes (GDE) can make gaseous CO_2 contact the catalyst and the electrolyte directly, thus shorten the path of dissolution and diffusion of CO_2 and make the reduction faster consequently. Prakash reported that a GDE prepared from commercial Sn powders and Nafion ionomer produces formic acid at a current density of 27 mA cm^{-2} (352 μmol h^{-1} cm^{-2}) with FE of approximately 70%;[18] by using a filter-press-type electrochemical cell, Castillo reported a GDE loaded with Sn particles produces formic acid at a current density of 40 mA cm^{-2} (522 μmol h^{-1} cm^{-2}) with FE of 70%[25] and a current density of 90 mA cm^{-2} (1175 μmol h^{-1} cm^{-2}) with FE of approximately 70% were obtained on a GDE loaded with 0.75 mg cm^{-2} of 150 nm Sn particles.[26]

It is well known that the hydrogen evolution reaction (HER) competes with CO_2 reduction,[27,28] and electrodes with high overpotential for HER can increase the FE for $ERCO_2$, electrodes with low overpotential for $ERCO_2$ are highly required to reduce the energy consumption. While maintaining FE (＞80%), Li fabricated an electrode (mesoporous SnO_2 nanosheets on carbon cloth) through a facile combination of hydrothermal reaction and calcination, and this electrode exhibits a partial current density of approximately 45 mA cm^{-2} (730 μmol h^{-1} cm^{-2}) at a moderate potential (−1.6 V *vs.* Ag/AgCl) with FE of 87%;[29] Kumar reported an electrochemically reduced SnO_2 porous nanowire catalyst with a high density of grain boundaries, this catalyst exhibits a partial current density of approximately 7 mA cm^{-2} (105 μmol h^{-1} cm^{-2}) with FE of 80% at approximately −1.4 V (*vs.* Ag/AgCl).[30] Considerable efforts have also been made to convert CO_2 by using a bimetallic catalyst,[31-37] especially for obtaining a formate product.[38-40] Choi reported a Sn–Pb alloy with surface composition $Sn_{56.3}Pb_{43.7}$, which exhibits the highest FE of 80% with the highest partial current density of 45.7 mA cm^{-2} (649 μmol h^{-1} cm^{-2}) at −2.0 V (*vs.* Ag/AgCl) for formate in an H-type cell;[38] Kortlever demonstrated that $Pd_{30}Pt_{70}$/C nanoparticles exhibited FE of 88%, average current density of 5 mA cm^{-2} (82 μmol h^{-1} cm^{-2}) at −1.0 V (*vs.* Ag/AgCl) for formate in an H-type cell.[40] The aforementioned studies have demonstrated that bimetallic catalysts can have a comparable or even higher catalytic activity towards formic acid formation compared with single metallic catalysts.

In order to improve on Sn material, it may be useful to couple to Sn an oxyphilic material, In, to obtain a catalyst that promotes the formation of formate at a relatively low overpotential with high

FE and current density. This could result in a more sluggish hydrogen evolution so that a low applied potential can be employed. In this work, different compositions of Sn–In catalyst were obtained and their catalytic activities were also studied.

2. EXPERIMENTAL

2.1. Synthesis and Preparation of Bimetallic Catalysts

Sn–In electrodes were prepared through electrodeposition on Cu foam (99.99%) by using a conventional three-electrode cell with a volume of 30 mL at 298 K under atmospheric pressure. Before an experiment, the Cu foam was treated in 8% dilute sulphuric acid with an ultrasonic bath for 10 min to remove impurities on the surface, after which the Cu foam was exposed to an electrodeposition bath with 1 cm^2 area by masking the other part with an epoxy resin. A Pt foil with 1 cm^2 surface area and Ag/AgCl filled with saturated KCl were used for the counter and reference electrodes, respectively. The electrodeposition bath was prepared by the addition of $Sn(CH_3COO)_2$ (Sigma-Aldrich, 99.9%) and $In(CH_3COO)_3$ (Sigma-Aldrich, 99.9%) to aqueous CH_3COOH solution of an approximately pH of 2.50, which was prepared from 36% (w/w) CH_3COOH (Kelong). The electrodeposition bath was bubbled using purified N_2 gas (99.9%) for at least 20 min before the experiment was begun, and this atmosphere was maintained during the experiment. The concentration of metal cation (Sn^{2+} or In^{3+}) in the electrolyte was 1.0 mM for all experiments. Four electrodes with different compositions (Sn_xIn_{100-x}) were obtained at varying potential through potentiostatic electrodeposition lasting 8 h. The prepared electrodes were rinsed with deionised water and dried at room temperature.

2.2. Material Characterisation

SEM and EDS were performed on a Pro-X desktop scanning electron microscope at an acceleration voltage of 15 kV. XRD patterns were recorded on an Ultima IV using Cu Kα radiation (1.54056 Å) and a scan range from 30° to 80°. XPS was performed on a Thermo ESCALAB 250XI. The characterization of the product is the same as the reported in our last article.[41]

2.3. Electrochemical Measurements

All electrochemical experiments were performed on a CorrTest CS350 electrochemical workstation. LSV measurements at a scan rate of 0.01 V s^{-1} and the $ERCO_2$ were obtained in the three-electrode cell, which was the same setup as in the electrodeposition experiment except for the type of electrolyte. The electrolyte used for LSV measurements was an aqueous solution of 0.1 M $KHCO_3$ saturated with N_2 (99.9%) or CO_2 (99.9%) prior to measurements. The electrolyte used for $ERCO_2$ was bubbled with CO_2 at 20 mL min^{-1} during the electrolysis. All experiments were performed under room temperature and ambient pressure.

3. RESULTS AND DISCUSSION

3.1. Preparation of Sn–In catalysts

Using Cu foam as the substrate and working electrode, the CV curves were performed in the solution of 1.0 mmol L^{-1} $Sn(CH_3COO)_2$ or $In(CH_3COO)_3$, whose pH was adjusted to 2.50 with CH_3COOH. The results are shown in Figure 1 with different potential ranges of −0.50~1.00, −0.75~1.00, −1.00~1.00, −1.25~1.00, and −1.50~1.00 V. Different potential scan ranges are used to study the characteristics of metal deposition.

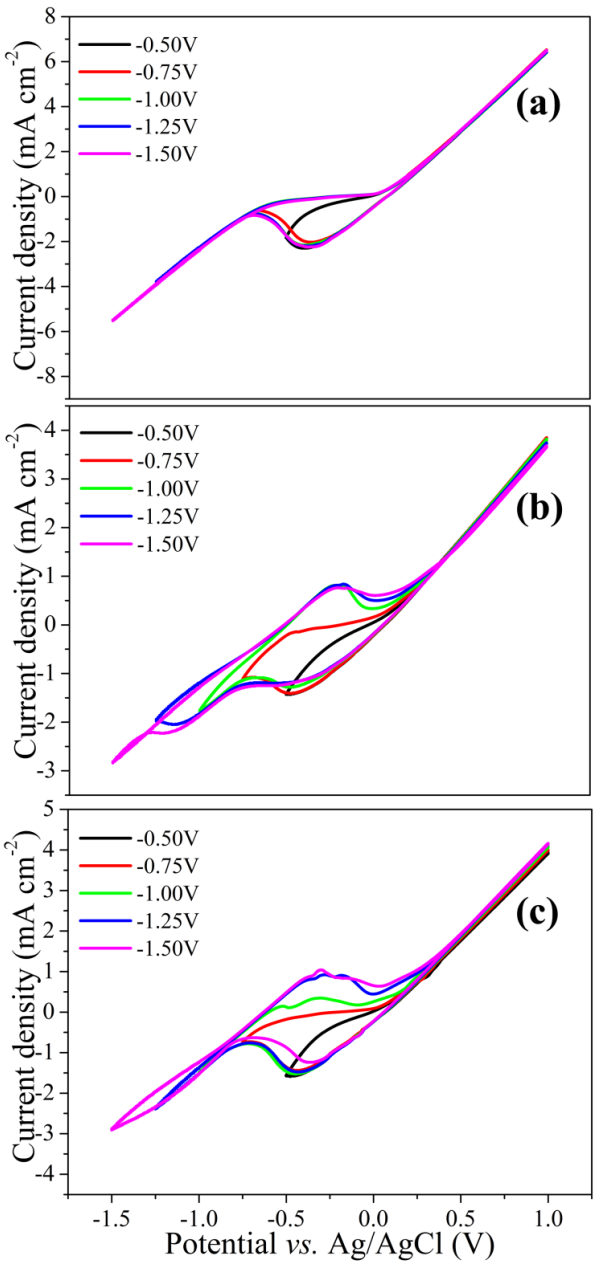

Figure 1. CV curves of Cu foam electrode in solution of (a) CH_3COOH; (b) $Sn(CH_3COO)_2$; and (c) $In(CH_3COO)_3$. $C_{(Sn^{2+} \text{ or } In^{3+})}$ = 1.0 mM, $pH_{solution}$ = 2.50.

Figure 1a shows the CV curves of Cu foam in CH_3COOH solution with pH = 2.50, which all have only one reduction peak at −0.36 V, corresponding to the reduction of copper oxide on surface. When the Cu foam was immersed in 1.0 mmol L^{-1} $Sn(CH_3COO)_2$ or $In(CH_3COO)_3$, the CV curves exhibit another broad reduction peak between −0.75 and −1.28 V (Figure 1b) , or −0.80 and −1.50 V (Figure 1c), and there is no oxidation peak if the potential scan range is −0.50~1.00 V or −0.75~1.00 V in both cases, therefore, the extra reduction peak comes from the electrodeposition of Sn or In, and the oxidation peak comes from the oxidation of metal. Consequently, we have electrodeposited Sn-In on Cu foam to obtain the Sn–In electrodes in N_2-purged 1.0 mM Sn^{2+} and In^{3+} solutions at potentials from −0.9 to −1.5 V.

3.2. Characterisations

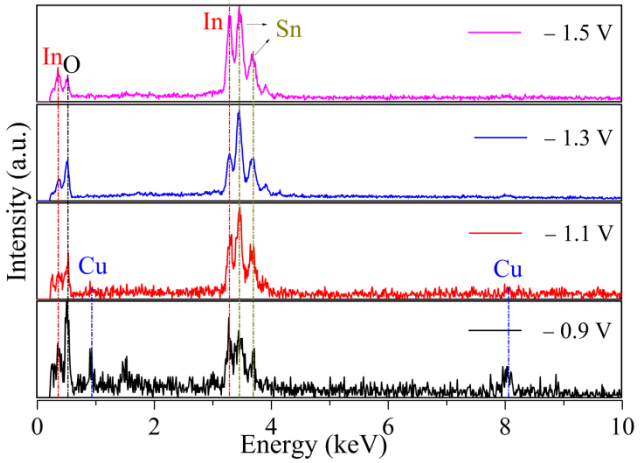

Figure 2. EDS of Sn–In catalysts produced using various deposition potentials.

Table 1. Atomic ratio data of Sn–In catalysts obtained using XPS.

Potential (V) / Atomic (%)	−0.9	−1.1	−1.3	−1.5
Cu	3.65	1.05	0	0
Sn	21.78	21.11	18.11	2.58
In	13.35	18.72	25.01	23.19
Sn:In	62:38	53:47	42:58	10:90

The compositions of the Sn–In electrodes were measured with EDS and XPS (Figure 2, Table 1). The data show that there are Sn, In and O on the surface of all electrodes. Cu is found in the electrodes deposited at potentials above −1.3 V, however the ratio of In of Sn–In electrodes increases

with more negative potential. To reflect the compositions of the samples, hereafter, the electrodes are identified with the atomic ratios of Sn and In calculated using the data in Table 1.

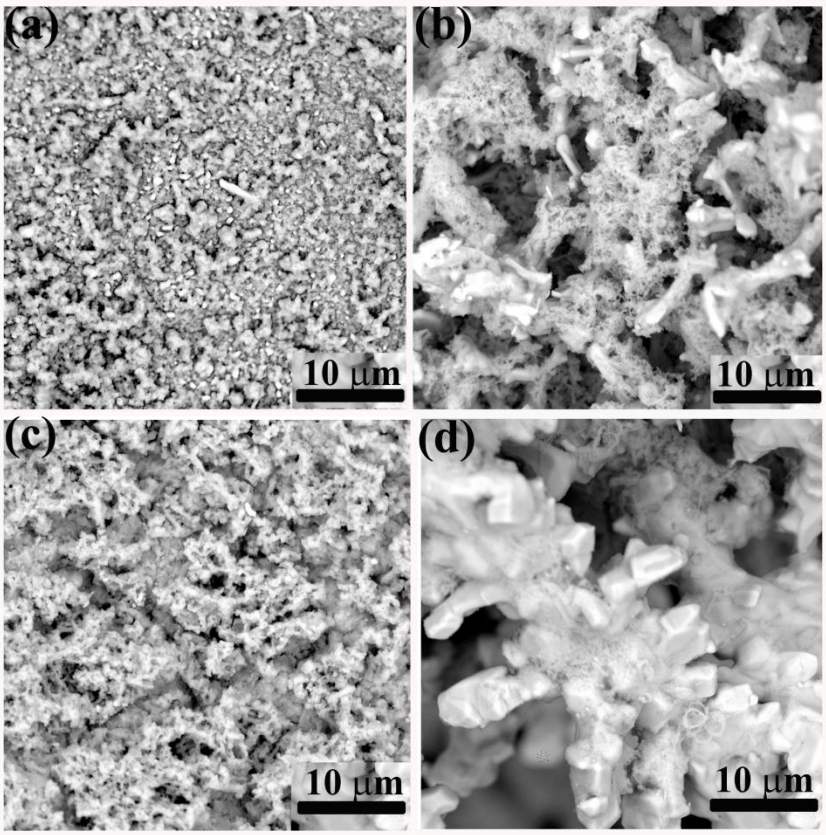

Figure 3. SEM images of electrodes obtained through electrodeposition with different compositions: (a) $Sn_{62}In_{38}$, (b) $Sn_{53}In_{47}$, (c) $Sn_{42}In_{58}$, and (d) $Sn_{10}In_{90}$.

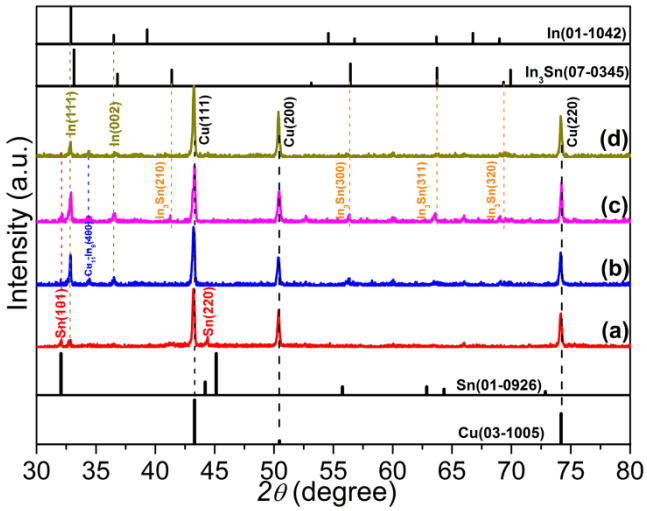

Figure 4. XRD patterns of the prepared electrodes with different compositions: (a) $Sn_{62}In_{38}$, (b) $Sn_{53}In_{47}$, (c) $Sn_{42}In_{58}$, and (d) $Sn_{10}In_{90}$.

Figure 3a shows that the $Sn_{62}In_{38}$ electrode has a closely packed granular structure. When the proportion of In increases, the dendritic structure becomes apparent (Figure 3b),[42] and specially in Figure 3c, it can be observed that the grains with size of 400 nm are dispersed on the dendritic structure, showing good permeability. For Sn:In atomic ratio of approximately 1:9 (Figure 3d; $Sn_{10}In_{90}$), it shows a thicker dendritic structure with little particles on.

Figure 4 shows the XRD patterns of prepared electrodes with Sn and In co-deposited. Cu(111), Cu(200), and Cu(220) can be identified in Figure 4a–4d because the deposition shell is thin and penetrable by X-rays. Reflections corresponding to both Sn and In are observed in the diffractograms (Figure 4a–4d), indicating that Sn and In were electrodeposited on the surface of the Cu foam. Except for the diffraction peak of Cu, the $Sn_{62}In_{38}$ electrode shows 3 reflections in the 2θ range investigated (Figure 4a), revealing a random distribution of crystals on the surface with preferential orientation in Sn(101), Sn(220), and In(111) directions. The $Sn_{53}In_{47}$ electrode shows reflections with preferential orientation in the In(002) and $Cu_{11}In_9$(400) directions[42,43] (Figure 4b). And for the $Sn_{42}In_{58}$ electrode, it has preferential orientation in the In_3Sn(210), In_3Sn(300), In_3Sn(311), and In_3Sn(320) directions in Figure 4c, indicating a structure of homogeneous dispersion of In_3Sn particles (as shown in Figure 3c).[44] In addition, the relative intensity of diffraction peaks of Sn and In was varied with Sn/In ratio, and the $Sn_{10}In_{90}$ electrode shows the diffraction peak of In is more conspicuous than that of Sn (Figure 4d).

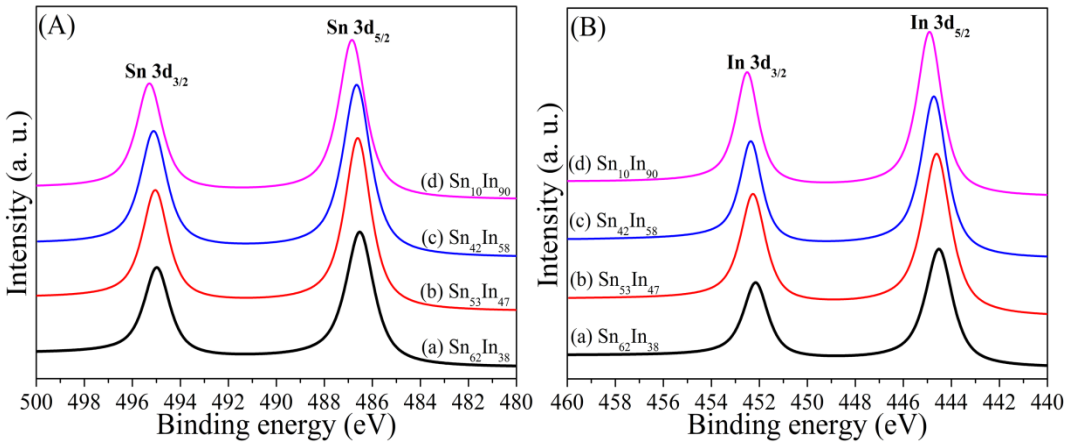

Figure 5. XPS spectra of (A) Sn 3d and (B) In 3d for Sn–In catalyst electrodes (a) $Sn_{62}In_{38}$, (b) $Sn_{53}In_{47}$, (c) $Sn_{42}In_{58}$, and (d) $Sn_{10}In_{90}$.

Table 2. Peak binding energies of Sn 3d and In 3d signals from prepared electrodes

	Sn 3d		In 3d	
electrode	Sn $3d_{3/2}$	Sn $3d_{5/2}$	In $3d_{3/2}$	In $3d_{5/2}$
$Sn_{62}In_{38}$	494.9	486.5	452.1	444.5
$Sn_{53}In_{47}$	495.0	486.6	452.2	444.6
$Sn_{42}In_{58}$	495.1	486.7	452.3	444.7
$Sn_{10}In_{90}$	495.3	486.9	452.5	444.9

XPS signals of Sn and In are presented in Figure 5, and the peak binding energies of the Sn and In signals are listed in Table 2. The binding energy has been corrected with the reference C 1s core level at 284.6 eV. The high-resolution Sn 3d peak of the prepared electrodes, presented in Figure 5A, is split into two strong peaks, which is in agreement with a report (Sn $3d_{3/2}$ and Sn $3d_{5/2}$ binding energies appear at 495.9 and 487.5 eV),[38] and a slight shift of Sn 3d signals with the composition of the catalysts were observed (Figure 5Aa–d, Table 2).[38,45,46] From the XPS spectra in Figure 5Ba, the In 3d peak is split into two strong peaks at 444.5 eV (In $3d_{5/2}$) and 452.1 eV (In $3d_{3/2}$), which is in agreement with a report on In_2O_3.[47,48] The In 3d signal undergoes a shift to high binding energy when the In ratio increases in the catalysts (Figure 5Ba–d); among the indium constituents, In_2O_3 was the dominant In species at the surface.[49,50]

3.3. Electrochemical Measurements

Figure 6 shows the LSV curves of the prepared electrodes in 0.1 M $KHCO_3$ under N_2 (black) and CO_2 (red) atmosphere. To investigate the actual electrochemical behaviour of the electrodes for $ERCO_2$, the scanning potential was varied from −1.1 to −2.0 V because metallic oxide on the surface of the electrode is reduced when the potential is lower than −1.1 V.[38]

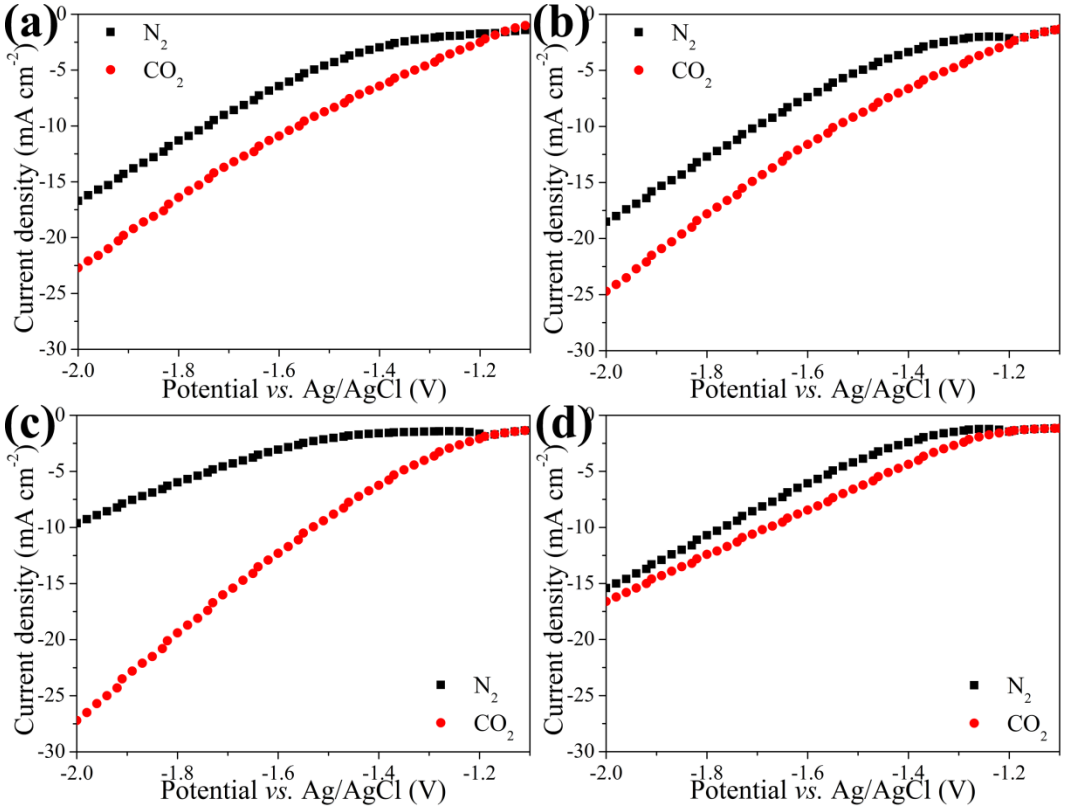

Figure 6. LSV curves recorded on the (a) $Sn_{62}In_{38}$, (b) $Sn_{53}In_{47}$, (c) $Sn_{42}In_{58}$, and (d) $Sn_{10}In_{90}$ electrodes in a 0.1 M $KHCO_3$ solution under N_2 (black) and CO_2 (red) atmosphere at potentials from −1.1 to −2.0 V (*vs.* Ag/AgCl) with a scan rate of 0.01 V s^{-1}.

At more negative potentials, sharp increases of the current densities can be observed under both N_2 and CO_2. Under N_2, this increase is due to the reduction of H_2O (HER); under CO_2, the enhanced current must be caused by the reduction of both H_2O and CO_2. The LSV curves in Figure 6a and 6b show that the $Sn_{62}In_{38}$ and $Sn_{53}In_{47}$ electrodes both have a certain catalytic activity for $ERCO_2$. However, for the $Sn_{42}In_{58}$ electrode in Figure 6c, the reduction current density under N_2 is higher while the reduction current density under CO_2 is lower than that for the electrodes (Figure 6a and 6b), which shows that it can effectively inhibit HER and improve the performance for $ERCO_2$.[41] Figure 6d reveals that the $Sn_{10}In_{90}$ electrode has negligible catalytic activity for $ERCO_2$ because of no large difference is found in the reduction current densities under N_2 and under CO_2.

3.4. Electrocatalytic Reduction of CO_2

The FE and STY of $HCOO^-$ obtained using the Sn–In electrodes were determined, and the results are presented in Figure 7.

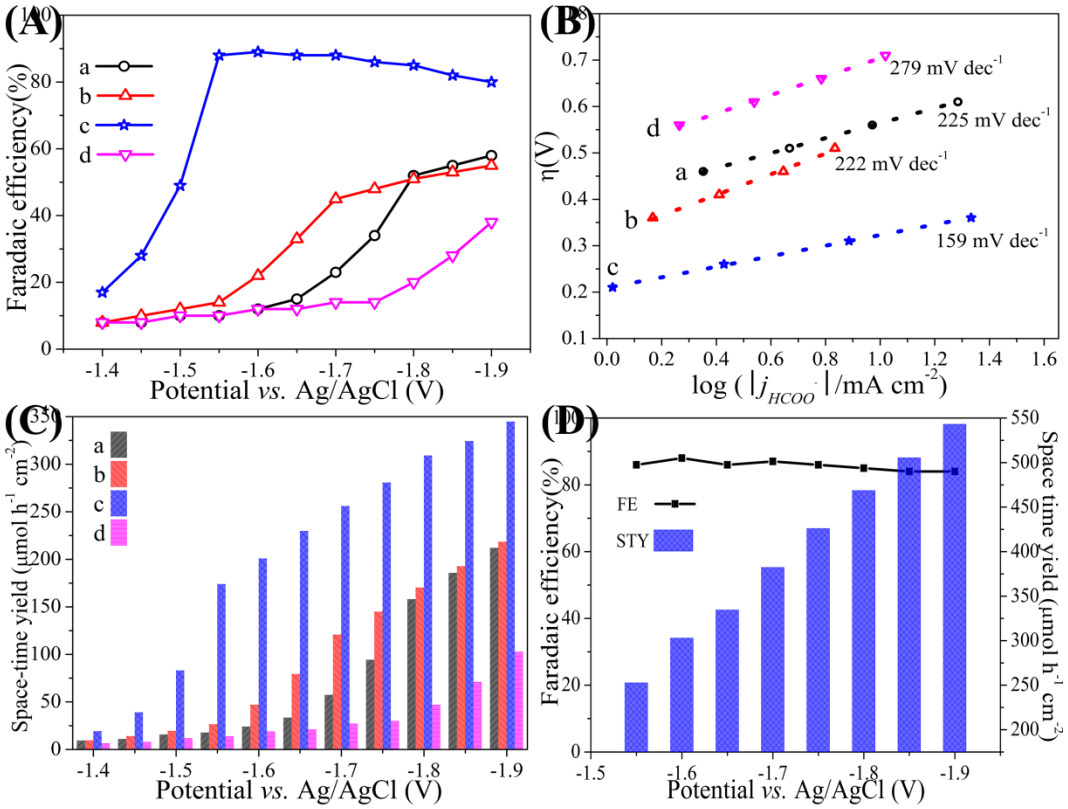

Figure 7. (A) FE versus electrolysis potential; (B) Tafel plot for the production of formate; and (C) STY versus electrolysis potential on the electrode of (a) $Sn_{62}In_{38}$, (b) $Sn_{53}In_{47}$, (c) $Sn_{42}In_{58}$, and (d) $Sn_{10}In_{90}$. (D) FE, and STY of the $Sn_{42}In_{58}$ electrode used in the biomimetic electrochemical cell.

Figure 7A shows that the highest FE obtained was 88% at –1.6 V with the $Sn_{42}In_{58}$ electrode, and then this efficiency decreases slowly (Figure 7Ac). Its FE is always higher than that of the other electrodes (Figure 7Aa, 7Ab, and 7Ad), which increase slowly with more negative potential.

Therefore, in terms of FE (Figure 7Ac) and current density (Figure 6c) of the $Sn_{42}In_{58}$ electrode, a higher STY can be obtained through decreasing the potential. The Tafel slope of $Sn_{42}In_{58}$ (Figure 7Bc) is only 159 mV decade^{-1}, much smaller than that of the other electrodes. A smaller Tafel slope is advantageous for practical applications because it results in a lower rate-limiting activation energy barrier and hence remarkably higher catalytic activity,[51] also indicating surface-area-independent enhancement of the intrinsic catalytic activity.[52] It can be seen that the FEs of the Sn–In electrodes increase with more negative potential (Figure 7C), however, the $Sn_{42}In_{58}$ electrode exhibits an absolutely superior STY (Figure 7Cc), 309 μmol h^{-1} cm^{-2} at −1.8 V versus Ag/AgCl, which is considerably higher than the yields previously reported.[23] Figure 7D shows FE, and STY when the $Sn_{42}In_{58}$ electrode was used in the biomimetic electrochemical cell; the experimental conditions employed were the optimal conditions investigated in the previous studies.[41] The results show that the FE is approximately 85% regardless of the potential and a higher STY (468 μmol h^{-1} cm^{-2}) at −1.8 V versus Ag/AgCl was attained.

4. CONCLUSION

Sn–In catalysts can be obtained through electrodeposition in the plating solution comprising $Sn(CH_3COO)_2$ and $In(CH_3COO)_3$, and a $Sn_{42}In_{58}$ electrode deposited at −1.3 V (versus Ag/AgCl) shows grains with size of 400 nm dispersed on the dendritic structure.

The $Sn_{42}In_{58}$ electrode exhibits excellent catalytic activity for $ERCO_2$ at a high potential, the highest Faraday efficiency of 88% is achieved at −1.6 V (versus Ag/AgCl) with a Tafel slope of only 159 mV decade^{-1}.

Its space time yield reaches 309 μmol h^{-1} cm^{-2} at −1.8 V and an even higher STY can be obtained by decreasing the applied potential. The resulting electrode can be employed in the biomimetic electrochemical cell to obtain formate at a higher STY (468 μmol h^{-1} cm^{-2} at −1.8 V). Based on these results, Sn–In catalysts are concluded to open up the possibility of highly selective, nontoxic, and low-energy-consumption catalysts for CO_2 reduction.

ACKNOWLEDGEMENTS
This work is partly supported by the Fundamental Research Funds for the Central Universities (3207047452), the Priority Academic Program Development of Jiangsu Higher Education Institutions and the Jiangsu Key Laboratory for Advanced Metallic Materials (BM2007204).

References

1. S. Solomon, G.K. Plattner, R. Knutti and P. Friedlingstein, *Proc. Natl. Acad. Sci. U. S. A.,* 106 (2009) 1704-1709.
2. J. Hansen, M. Sato, R. Ruedy, K. Lo, D.W. Lea and M. Medina-Elizade, *Proc. Natl. Acad. Sci. U. S. A.,* 103 (2006) 14288-14293.
3. R.J. Lim, M. Xie, M.A. Sk, J.M. Lee, A. Fisher, X. Wang and K.H. Lim, *Catal. Today,* 233 (2014) 169-180.

4. M. Bukhtiyarova, T. Lunkenbein, K. Kähler and R. Schlögl, *Catal. Lett.,* 147 (2017) 416-427.
5. A.S. Agarwal, Y. Zhai, D. Hill and N. Sridhar, *ChemSusChem,* 4 (2011) 1301-1310.
6. G.A. Olah, G.K. Prakash and A. Goeppert, *J. Am. Chem. Soc.,* 133 (2011) 12881-12898.
7. M. Pérez-Fortes, J.C. Schöneberger, A. Boulamanti and E. Tzimas, *Appl. Energ.,* 161 (2016) 718-732.
8. D.R. Kauffman, J. Thakkar, R. Siva, C. Matranga, P.R. Ohodnicki, C. Zeng and R. Jin, *ACS Appl. Mater. Interfaces,* 7 (2015) 15626-15632.
9. N.S. Spinner, J.A. Vega and W.E. Mustain, *Catal. Sci. Technol.,* 2 (2012) 19-28.
10. A.M. Appel, J.E. Bercaw, A.B. Bocarsly, H. Dobbek, D.L. DuBois, M. Dupuis, J.G. Ferry, E. Fujita, R. Hille, P.J. Kenis, C.A. Kerfeld, R.H. Morris, C.H. Peden, A.R. Portis, S.W. Ragsdale, T.B. Rauchfuss, J.N. Reek, L.C. Seefeldt, R.K. Thauer and G.L. Waldrop, *Chem. Rev.,* 113 (2013) 6621-6658.
11. J. Qiao, Y. Liu, F. Hong and J. Zhang, *Chem. Soc. Rev.,* 43 (2014) 631-675.
12. J. Ma, N. Sun, X. Zhang, N. Zhao, F. Xiao, W. Wei and Y. Sun, *Catal. Today,* 148 (2009) 221-231.
13. B. Innocent, D. Liaigre, D. Pasquier, F. Ropital, J.M. Leger and K.B. Kokoh, *J. Appl. Electrochem.,* 39 (2009) 227-232.
14. A.M. Bartrom, J. Ta, T.Q. Nguyen, J. Her, A. Donovan and J.L. Haan, *J. Power Sources,* 229 (2013) 234-238.
15. J. Jiang and A. Wieckowski, *Electrochem. Commun.,* 18 (2012) 41-43.
16. N.V. Rees and R.G. Compton, *J. Solid State Electrochem.,* 15 (2011) 2095-2100.
17. X. Yu and P.G. Pickup, *J. Power Sources,* 182 (2008) 124-132.
18. G.K.S. Prakash, F.A. Viva and G.A. Olah, *J. Power Sources,* 223 (2013) 68-73.
19. M. Grasemann and G. Laurenczy, *Energ. Environ. Sci.,* 5 (2012) 8171.
20. Y. Hori, H. Wakebe, T. Tsukamoto and O. Koga, *Electrochim. Acta,* 39 (1994) 1833-1839.
21. W. Lv, R. Zhang, P. Gao and L. Lei, *J. Power Sources,* 253 (2014) 276-281.
22. W. Lv, J. Zhou, F. Kong, H. Fang and W. Wang, *Int. J. Hydrogen Energy,* 41 (2016) 1585-1591.
23. Y. Wang, J. Zhou, W. Lv, H. Fang and W. Wang, *Appl. Surf. Sci.,* 362 (2016) 394-398.
24. R. Zhang, W. Lv and L. Lei, *Appl. Surf. Sci.,* 356 (2015) 24-29.
25. A. Del Castillo, M. Alvarez-Guerra and A. Irabien, *AIChE Journal,* 60 (2014) 3557-3564.
26. A. Del Castillo, M. Alvarez-Guerra, J. Solla-Gullón, A. Sáez, V. Montiel and A. Irabien, *Appl. Energ.,* 157 (2015) 165-173.
27. C.H. Lee and M.W. Kanan, *ACS Catal.,* 5 (2014) 465-469.
28. Y.J. Zhang, V. Sethuraman, R. Michalsky and A.A. Peterson, *ACS Catal.,* 4 (2014) 3742-3748.
29. F. Li, L. Chen, G.P. Knowles, D.R. MacFarlane and J. Zhang, *Angew. Chem., Int. Ed.,* 56 (2017) 505-509.
30. B. Kumar, V. Atla, J.P. Brian, S. Kumari, T.Q. Nguyen, M. Sunkara and J.M. Spurgeon, *Angew. Chem., Int. Ed.,* 129 (2017) 3699-3703.
31. G.O. Larrazábal, A.J. Martín, S. Mitchell, R. Hauert and J. Pérez-Ramírez, *ACS Catal.,* 6 (2016) 6265-6274.
32. S. Sarfraz, A.T. Garcia-Esparza, A. Jedidi, L. Cavallo and K. Takanabe, *ACS Catal.,* 6 (2016) 2842-2851.
33. J. Christophe, T. Doneux and C. Buess-Herman, *Electrocatalysis,* 3 (2012) 139-146.
34. M. Alvarez-Guerra, A. Del Castillo and A. Irabien, *Chem. Eng. Res. Des.,* 92 (2014) 692-701.
35. F. Jia, X. Yu and L. Zhang, *J. Power Sources,* 252 (2014) 85-89.
36. S. Rasul, D.H. Anjum, A. Jedidi, Y. Minenkov, L. Cavallo and K. Takanabe, *Angew. Chem., Int. Ed.,* 54 (2015) 2146-2150.
37. G.O. Larrazábal, A.J. Martín, S. Mitchell, R. Hauert and J. Pérez-Ramírez, *J. Catal.,* 343 (2016) 266-277.
38. S.Y. Choi, S.K. Jeong, H.J. Kim, I.H. Baek and K.T. Park, *ACS Sustainable Chem. Eng.,* 4 (2016) 1311-1318.

39. D. Kim, J. Resasco, Y. Yu, A.M. Asiri and P. Yang, *Nat. Commun.,* 5 (2014) 4948.
40. R. Kortlever, I. Peters, S. Koper and M.T.M. Koper, *ACS Catal.,* (2015) 3916-3923.
41. F. Li, Z. Fan, J. Tai, H. Wei, Y. Zhou and L. Lei, *Ind. Eng. Chem. Res.,* 57 (2018) 12307-12313.
42. Z.B. Hoffman, T.S. Gray, K.B. Moraveck, T.B. Gunnoe and G. Zangari, *ACS Catal.,* 7 (2017) 5381-5390.
43. D. Liang, B. Unveroglu and G. Zangari, *J. Electrochem. Soc.,* 161 (2014) D613-D619.
44. W.J. Dong, C.J. Yoo and J.L. Lee, *ACS Appl. Mater. Interfaces,* 9 (2017) 43575-43582.
45. P.A. Grutsch, M.V. Zeller and T.P. Fehlner, *Inorg. Chem.,* 12 (1973) 1431-1433.
46. P. Simon, N. Bui, F. Dabosi, G. Chatainier and M. Provincial, *J. Power Sources,* 52 (1994) 31-39.
47. S.K. Poznyak and A.I. Kulak, *Electrochim. Acta,* 45 (2000) 1595-1605.
48. J.N. Tiwari, W.G. Lee, S. Sultan, M. Yousuf, A.M. Harzandi, V. Vij and K.S. Kim, *ACS Nano,* 11 (2017) 7729-7735.
49. P. Meriaudeau, *J. Catal.,* 152 (1995) 313-321.
50. R.L. Barbosa, V. Papaefthimiou, Y.T. Law, D. Teschner, M. Hävecker, A. Knop-Gericke, R. Zapf, G. Kolb, R. Schlögl and S. Zafeiratos, *J. Phys. Chem. C,* 117 (2013) 6143-6150.
51. F. Lei, W. Liu, Y. Sun, J. Xu, K. Liu, L. Liang, T. Yao, B. Pan, S. Wei and Y. Xie, *Nat. Commun.,* 7 (2016) 12697.
52. B. Kumar, V. Atla, J.P. Brian, S. Kumari, T.Q. Nguyen, M. Sunkara and J.M. Spurgeon, *Angew. Chem., Int. Ed.,* 56 (2017) 3645-3649.